Key Points:

- The timescales for local, vertical and lateral processes that regulate bottom oxygen are defined and quantified
- Comparable deficit and lateral exchange timescales under short local consumption timescale cause transient hypoxia
- Relatively longer lateral exchange timescale under short local consumption timescale favors long-lasting hypoxia

Correspondence to:
W. Zhang,
wenxia.zhang@sklec.ecnu.edu.cn

Using Timescales of Deficit and Residence to Evaluate Near-Bottom Dissolved Oxygen Variation in Coastal Seas

Wenxia Zhang[1,2] [ORCID], **John P. Dunne**[3] [ORCID], **Hui Wu**[1] [ORCID], **Feng Zhou**[2] [ORCID], and **Daji Huang**[4] [ORCID]

[1]State Key Laboratory of Estuarine and Coastal Research, East China Normal University, Shanghai, China, [2]State Key Laboratory of Satellite Ocean Environment Dynamics, Second Institute of Oceanography, Ministry of Natural Resources, Hangzhou, China, [3]Geophysical Fluid Dynamics Laboratory, National Oceanic and Atmospheric Administration, Princeton, NJ, USA, [4]Guangxi Key Laboratory of Beibu Gulf Marine Resources, Environment and Sustainable Development, Fourth Institute of Oceanography, Ministry of Natural Resources, Beihai, China

Abstract We identify the local, vertical and lateral processes that cause bottom oxygen variation, and characterize timescales for each process using oxygen budget analysis based on a coupled physical-biogeochemical model for the coastal seas in east China. Local oxygen deficit often occurs in the summer season due to the faster local consumption than the vertical replenishment in seasonal timescale. Lateral transport of oxygen-rich ambient water replenishes local deficit of bottom dissolved oxygen. Competition between local deficit and lateral exchange determines seasonal hypoxia formation and sustainment. Short local consumption timescale is favorable for hypoxia formation, and transient hypoxia often forms when the local deficit and lateral exchange processes act on comparable timescales, such as the East China Sea in which the bottom hypoxia usually lasts for days. Extremely long lateral exchange timescale suggests that dissolved oxygen variation is predominantly controlled by local processes, and short local consumption timescale often causes increasingly severe seasonal hypoxia until the onset of the relaxation of local deficit, such as the bottom hypoxia in the Bohai Sea. Using these timescales to evaluate local deficit relative to vertical and lateral residence time and their variability is a convenient and potentially powerful general mechanistic framework to evaluate strategies to mitigate coastal hypoxia worldwide.

Plain Language Summary Coastal hypoxia, usually defined as aquatic dissolved oxygen concentration lower than 63 mmol m^{-3}, has been a growing problem worldwide. Hypoxia causes detrimental effects and interrupts ecosystem functions, such as degradation of biodiversity, compression of habitat, and shrink of fish stock. Dissolved oxygen variation attributes to local oxygen consumption via biogeochemical process like degradation of organic matter, vertical replenishment via physical processes, and lateral exchange via horizontal advection. This study investigates coastal hypoxia from the perspective of timescale since these processes regulate dissolved oxygen on different timescales to compare different processes, evaluate bottom hypoxia sustainment, and isolate the relative importance of local and vertical, and lateral processes in hypoxia formation. We find this framework to have important implications for the comparative effectiveness of local ecosystem protection measures.

1. Introduction

Seasonal bottom dissolved oxygen stress occurs in both the open ocean and coastal seas (Breitburg et al., 2018; Rabalais et al., 2010). In the coastal seas, the rate of oxygen decrease is significantly accelerated by anthropogenic eutrophication (Conley et al., 2009, 2011; Rabalais et al., 2001, 2002), which leads to severe oxygen consumption at the near-bottom layer by microbial degradation of organic matter either sinking from high primary production at the surface/subsurface or transported from rivers (Najjar et al., 2018). Coastal seas with riverine inputs of freshwater and massive organic material and/or nutrients are especially vulnerable to seasonal oxygen decrease because organic matter decomposition causes oxygen consumption at the bottom water (e.g., Conley et al., 2011) while the supply of oxygen from the surface is concurrently inhibited by the strong vertical stratification associated with heat and freshwater inputs. Severe bottom hypoxia (dissolved oxygen, DO < 63 mmol m^{-3}) is often detected in summer (June, July, and August) in such regions like the north Gulf of Mexico (Rabalais et al., 2001, 2002), the Chesapeake Bay (Hagy et al., 2004; Murphy et al., 2011), the Baltic Sea (Carstensen et al., 2014; Conley et al., 2009, 2011), and the East China Sea (Chen et al., 2007). Summer bottom oxygen also
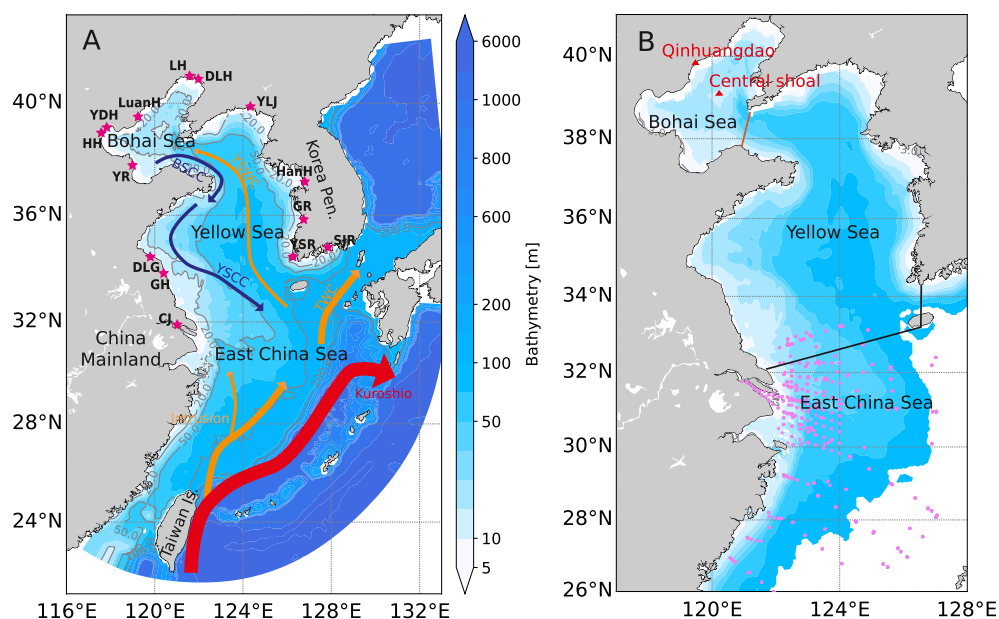
Figure 1. (a) The entire model domain, in which the paths of the Kuroshio current, the Kuroshio subsurface water intrusion are denoted. The circulation pattern in the coastal and shelf water is briefly marked. The red stars denote the locations of multiple rivers that introduce both freshwater and nutrients into the study domain. The abbreviations of the currents are for Tsushima Warm Current (TWC), Yellow Sea Coastal Current (YSCC), Yellow Sea Warm Current (YSWC), and Bohai Sea Coastal Current (BSCC). The abbreviations of the rivers are for Changjiang River (CJ), Guanhe River (GH), Doulonggang River (DLG), Yellow River (YR), Haihe River (HH), Yongdinghe River (YDH), Luanhe River (LuanH), Liaohe River (LH), Daliaohe River (DLH), Yalvjiang River (YLJ), Hanhe River (HanH), Geum River (GR), Youngsan River (YSR), and Seomjin River (SJR). The gray lines are 20, 50, 100, and 200 m isobath. (b) The subregions that selected for oxygen budget analysis. Note that the pink marks are observation stations during cruises as listed in Table 1, and region deeper than 100 m is blanked.

shows rapid decline and approaches hypoxia in recent years in the Bohai Sea (Song et al., 2020; Wei et al., 2019), a shallow and semi-closed sea in northeast China.

The variation in bottom dissolved oxygen is generally controlled by a combination of local consumption, vertical replenishment, and lateral exchange with adjacent regions. Local consumption is primarily caused by the degradation of organic matter; metabolism of oceanic organism also contributes to the consumption of dissolved oxygen (Fennel et al., 2013; Yu et al., 2015). Vertical replenishment is driven by physical processes (vertical diffusion and convection) associated with wind driven-mixing and winter overturning that supply oxygen from surface to bottom (Ni et al., 2016; Zhang et al., 2018; Zhou et al., 2017). Lateral exchange is dominated by horizontal advection with the overall influence characterized by the coastal water residence time, the time required to replace water mass in a certain coastal region with (typically higher oxygen) waters from the ambient. The residence time is highly linked with local geomorphology, for instance, semi-closed regions like the Bohai Sea and the Chesapeake Bay have restricted exchange with adjacent regions, and are associated with pronouncedly long water residence time (Liu et al., 2019; Takeoka, 1984).

This study puts forward definitions of rates and timescales for different processes that regulate bottom oxygen concentration based on oxygen budget analysis. The East China Sea, different from the semi-closed Bohai Sea, has direct connection with the open ocean (Figure 1a). Thus, these coastal seas in east China are investigated as a contrasting prototype, and the rates and timescales for bottom oxygen variation are quantified and compared among seas (subregions hereafter, Figure 1b) based on a coupled physical-biogeochemical model. The quantification and comparisons of these timescales are then used to isolate the relative importance of local and vertical, and lateral processes in varying bottom oxygen concentration, which have important implications for the potential effectiveness of local ecosystem protection measures.

Table 1
Research Cruises in the East China Sea During Years 2011–2017 Referred to in This Study

Cruise number and season	Time	Research vessel	Total sampling number
1 Summer	11–29 August 2011	R/V *Beidou*	69
2 Spring	8–19 May 2013	R/V *Beidou*	39
3 Summer	6–28 August 2013	R/V *Beidou*	78
4 Fall	12 October to 6 November 2013	R/V *Beidou*	34
5 Summer	4–15 July 2016	R/V *Runjiang*	75
6 Summer	19–28 July 2016	R/V *Runjiang*	87
7 Summer	20 July to 2 August 2017	R/V *Runjiang*	88

2. Methodology

2.1. Observation

In-situ observational measurements used here for model validation were obtained aboard the R/Vs *Beidou*, and *Runjiang* during several cruises from 2011 to 2017 conducted in the East China Sea. A summary of the cruises with start and end dates is given in Table 1. Discrete dissolved oxygen concentration measurements were obtained using a conventional Winkler titration (Bryan et al., 1976) of water samples during cruises off the Changjiang River estuary and the adjacent East China Sea in 2011, 2013, 2016, and 2017. Depths for the collection of water samples were decided at each location on the basis of the recorded CTD profile, which usually included a surface sample (approximately 2 ∼ 3 m underneath the free surface), a bottom sample (3 ∼ 5 m above the seabed), samples both above and below the pycnocline, and additional samples accordingly in consideration of the water column depth.

Satellite-derived daily chlorophyll concentration and high-resolution monthly sea surface temperature were obtained from the Geostationary Ocean Color Imager Level 2 product (GOCI, https://oceandata.sci.gsfc.nasa.gov/GOCI/L2/) and Moderate Resolution Imaging Spectroradiometer (MODIS, https://oceandata.sci.gsfc.nasa.gov/MODIS-Aqua/Mapped/Monthly/4km), respectively.

2.2. Model Description

This study used the hydrodynamic model based on Regional Ocean Modeling System (ROMS), Shchepetkin and McWilliams (2005) and coupled with a biological model. The hydrodynamic model domain (Figure 1a) encompasses the entire Bohai Sea, Yellow Sea, East China Sea, and part of the Japan Sea and deep region offshore. The model in this study expanded that in Zhang et al. (2018; 2019; 2021) to include 10 rivers along the coast of China (http://www.mwr.gov.cn/), and 4 rivers along the coast of Korea Peninsula (Kim et al., 2013) (Figure 1a). This ROMS-based model has 30 vertical layers, with a minimum water depth of 3 m and a maximum depth of slightly greater than 7,000 m. The horizontal resolution ranges from <500 m in the upper estuary, to ∼1 km in the plume near-field region, and to ∼2 km in the offshore region. The model run was initiated from rest and was forced with surface momentum and heat fluxes from the European Center for Medium-Range Weather Forecasts (ECMWF, https://www.ecmwf.int/en/forecasts/datasets), freshwater flux, and current and tide at the open boundary. The initial and open boundary conditions for physical component are extracted from World Ocean Atlas 2013 (WOA13, https://www.nodc.noaa.gov/OC5/woa13/), and monthly Simple Ocean Data Assimilation (SODA, https://climatedataguide.ucar.edu/climate-data/soda-simple-ocean-data-assimilation), respectively. 13 tidal constituents (MM, MF, Q1, O1, P1, K1, N2, M2, S2, K2, MN4, M4, and MS4) are imposed based on tidal elevations and currents extracted from the global inverse tide model TPXO7.2 of Oregon State University (Egbert & Erofeeva, 2002).

The biological component is a nitrogen cycle model (Fennel et al., 2013) expanded to include dynamics of DIP (Dissolved Inorganic Phosphorus) (Laurent et al., 2017), which includes two species of dissolved inorganic nitrogen (nitrate, NO_3, and ammonium, NH_4), DIP (phosphate, PO_4), one functional phytoplankton group (Phy), chlorophyll (Chl) as a separate state variable, one functional zooplankton group (Zoo), two pools of detritus representing large, fast-sinking particles (LDet) and suspended, small particles (SDet), and dissolved oxygen (DO) as a state variable (Figure 2). The equation of dissolved oxygen budget is given as

$$\int \frac{\partial Ox}{\partial t} dV = -\int \left(u\frac{\partial Ox}{\partial x} + v\frac{\partial Ox}{\partial y} + w\frac{\partial Ox}{\partial z} \right) dV + \int \left[\frac{\partial}{\partial x}\left(K_H \frac{\partial Ox}{\partial x} \right) + \frac{\partial}{\partial y}\left(K_H \frac{\partial Ox}{\partial y} \right) \right.$$
$$\left. + \frac{\partial}{\partial z}\left(K_V \frac{\partial Ox}{\partial z} \right) \right] dV + PP + WCR + Nitrif + F_{SOD} + F_{air-sea}. \tag{1}$$

Note that all the budget terms are provided by direct model output and then integrated over the corresponding subregions to achieve dissolved oxygen budget. *Ox* represents dissolved oxygen concentration (mmol m^{-3}), *dV* is the volume of a model grid cell (m^3). The first two budget terms on the right-hand side are advection and
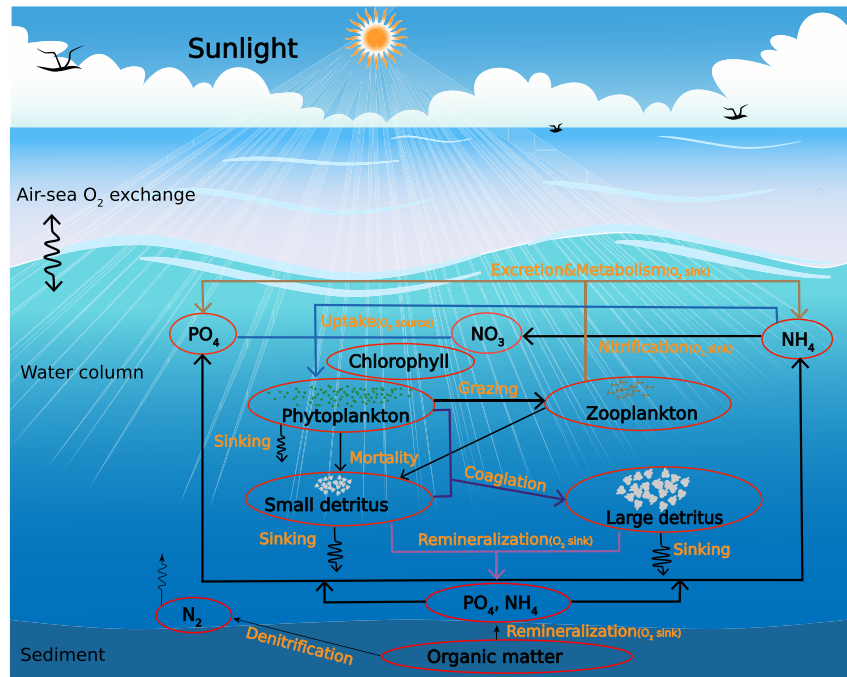
Figure 2. Schematic of the biogeochemical model representing ecosystem processes and pathways. Biogeochemical processes that produce and consume dissolved oxygen (O_2) are indicated with O_2 source and sink, respectively.

diffusion-induced oxygen changes, respectively, which are direct output of the model. In these terms x, y, and z represent the two horizontal coordinates and the vertical coordinate, respectively; u, v, and w represent velocity components in x, y, and z coordinates, respectively; K_H and K_V are the horizontal and vertical diffusivities (m^2 s^{-1}), respectively. The term PP is primary production

$$PP = \int \mu_{\max}(T) f(E) \left(\frac{L_{NO_3}}{L_N} R_{O_2:NO_3} + \frac{L_{NH_4}}{L_N} R_{O_2:NH_4} \right) \min(L_N, L_P) Phy \, dV, \tag{2}$$

WCR is water column respiration

$$WCR = -\int R_{O_2:NH_4} \left(l_{BM} Zoo + l_E \frac{Phy^2}{k_P + Phy^2} \beta Zoo + \hat{r}_{SD}^N SDet + \hat{r}_{LD}^N LDet \right) dV, \tag{3}$$

and $Nitrif$ stands for oxygen consumption due to nitrification

$$Nitrif = -\int 2R_{O_2:NH_4} \hat{n} NH_4 \, dV, \tag{4}$$

where $\mu_{\max} = \mu_0 \times 1.066^T$ (Eppley, 1972) is the maximum growth rate of phytoplankton (day^{-1}), and $f(E) = \frac{\alpha E}{\sqrt{\mu_{\max}^2 + \alpha^2 E^2}}$ (Evans & Parslow, 1985) is light limitation. The intensity of photosynthetic available radiation at depth z, E, is parameterized following Fennel et al. (2011)

$$E = E_0 \cdot PAR \cdot \exp \left(-AttSW \cdot z - AttSed \cdot z - AttChl \cdot \int_0^z Chl(\xi) d\xi \right), \tag{5}$$

where E_0 is the net solar shortwave radiation at the surface, and PAR is the fraction of photosynthetic available radiation to the shortwave radiation. $AttSed$ is parameterized light attenuation caused by sediment. Upper estuary is extremely turbid due to the huge amount of sediment flux from the Changjiang and Yellow Rivers, and $AttSed = 0.7$ (salinity < 26); 0.05 (salinity > 26). The 26 isohaline was selected according to the turbidity distribution in the upper estuary of the Changjiang River (Wang et al., 2019) which showed that phytoplankton bloom occurred at the offshore edge of the high turbidity zone. Light attenuation due to seawater ($AttSW$) and

Chlorophyll (*AttChl*) are 0.04 m^{-1} and 0.024 86 (mg Chl m^2)$^{-1}$, respectively. Nutrient limitation factors for nitrogen and phosphorus are

$$L_{NO_3} = \frac{NO_3}{k_{NO_3} + NO_3} \cdot \frac{1}{1 + NH_4/k_{NH_4}}, \tag{6}$$

$$L_{NH_4} = \frac{NH_4}{k_{NH_4} + NH_4}, \tag{7}$$

$$L_N = L_{NO_3} + L_{NH_4}, \tag{8}$$

$$L_P = \frac{DIP}{k_{DIP} + DIP}. \tag{9}$$

The rest of the biological parameters are kept identical as those used in Zhang et al. (2018), and the readers are referred to Zhang et al. (2018) for the list of the biological parameters.

F_{SOD} and $F_{air-sea}$ (in units of mmol day^{-1}) are the areal integral of oxygen fluxes across the bottom and the air-sea interface, respectively. The biological model specifies sediment oxygen demand (SOD) as a negative flux of oxygen at the seafloor based on bottom temperature and oxygen concentrations (Hetland & DiMarco, 2008), and the areal integral of the flux is

$$F_{SOD} = \int 6.0 \left[\text{mmol m}^{-2}\text{day}^{-1}\right] \times 2^{T/10.0°C} \times \left[1 - \exp\left(-\frac{Ox}{30.0 \text{ mmol m}^{-3}}\right)\right] dS; \tag{10}$$

the areal integral of gas exchange across the air-sea interface is parameterized as

$$F_{air-sea} = \int \frac{v\kappa_{O_2}}{\Delta z}(Ox_{sat} - Ox)dS, \tag{11}$$

where dS is the area of a model grid cell, $v\kappa_{O_2}$ is the gas exchange coefficient for oxygen (Wanninkhof, 2014), and Ox_{sat} is oxygen concentration at saturation calculated following Garcia and Gordon (1992).

The initial and open boundary conditions for nutrients were extracted from the climatological monthly WOA13. The Changjiang riverine nutrient concentration was taken from Gao et al. [2012], the riverine nutrient concentrations for the other 9 rivers along the coast of China were taken from the Bulletin of China Marine Environment (http://english.mee.gov.cn), and the riverine nutrient concentrations for the 4 rivers along the coast of Korea Peninsula were taken from Kim et al. (2013). This model was initiated in January 2009 and ran for 9 years, and 4-hourly model output since 2011 was analyzed to ensure sufficient spin-up. Except for the model-observation comparison, only model output for 2011–2015 were analyzed and averaged considering the time consuming process of the analysis of the vast amounts of model output. The East China Sea subregion is selected as the region shallower than 100 m between 26-33°N, because the Changjiang River introduced freshwater and massive nutrient loads have the most pronounced impacts in this region.

2.3. Variation Rates and Timescales

Oxygen budget analysis is done for the entire water column, for the upper layer (upper 70% of the water column), and for the lower layer (lower 30% of the water column). The bottom boundary layer is a near-bottom layer that can be directly affected by the drag of currents on the seafloor (Zhang et al., 2020). A thin bottom boundary layer often forms under the intensified stratification, which acts to promote rapid development of bottom hypoxia (Wiseman et al., 1997). Model results indicate that the thickness of the bottom boundary layer accounts for an average of 28% of the water column depth over the shelf. Thus, the lower 30% of the water column was selected to represent the lower layer. The choice of the critical value used to define the lower layer will affect the exact value of the budget terms. However, qualitatively different reasonable choices for the critical value (i.e., thinner lower layer) will yield the same result. The lower layer is paid close attention because summer hypoxia is generally confined within this layer. The dissolved oxygen consumption in the lower layer is caused by local biogeochemical processes (*WCR*, *Nitrif*, F_{SOD} and *PP*). The local oxygen consumption rate in the lower layer (R'_c, mmol day^{-1}) is defined as

$$R'_c = WCR + Nitrif + F_{SOD} + PP. \tag{12}$$

It is worth mentioning that PP is generally trivial in the lower layer and often negligible. Hence, the supply of oxygen by primary production at the bottom is negligible. The vertical replenishment of dissolved oxygen in the lower layer is controlled by $VAdv = -\int w \frac{\partial Ox}{\partial z} dV$, and $VDiff = \int \frac{\partial}{\partial z} \left(K_V \frac{\partial Ox}{\partial z} \right) dV$. Thus, the vertical oxygen replenishment rate (R'_r, mmol day^{-1}) is defined as

$$R'_r = VAdv + VDiff. \tag{13}$$

Then, the local oxygen deficit rate (R'_d, mmol day^{-1}), the sum of the local consumption rate and the vertical replenishment rate, is defined as

$$R'_d = R'_c + R'_r = (WCR + Nitrif + F_{SOD} + PP) + (VAdv + VDiff). \tag{14}$$

The horizontal advection process is considered as the lateral exchange process (horizontal diffusion term is trivial and neglected), an adjacent impact, between one region and another to relax local oxygen deficit. Thus, the lateral oxygen exchange rate (R'_e, mmol day^{-1}) is defined as

$$R'_e = HAdv = -\int \left(u \frac{\partial Ox}{\partial x} + v \frac{\partial Ox}{\partial y} \right) dV. \tag{15}$$

These rates are then normalized by the area of the corresponding subregion to obtain the normalized rates, and the normalized rates (in units of mmol m^{-2} day^{-1}) are written as R_c, R_r, R_d, and R_e, respectively. The competition between the local oxygen deficit and the lateral exchange determines the net oxygen variation, and persistent oxygen loss facilitates the formation of bottom hypoxia. The timescales for local consumption and deficit (τ_c and τ_d, day) are defined as the time required for these processes to bring water oxygen in a subregion from background-level to hypoxic condition (DO < 63 mmol m^{-3}), and the timescales for vertical replenishment and lateral exchange (τ_r and τ_e, day) are defined as the time required for these processes to bring water oxygen in a subregion from hypoxic condition (DO < 63 mmol m^{-3}) to background-level. Note the background-level oxygen concentration is the summer-averaged oxygen concentration in the lower layer.

2.4. The Calculation of Vertical Stratification

The Brunt-Väisälä frequency, N, is often used to denote the strength of stratification (Brunt, 1927), which is defined as

$$N^2 = -\frac{g}{\rho_0} \frac{\partial \rho}{\partial z}, \tag{16}$$

where $g = 9.8$ m s^{-2} is the gravitational acceleration; ρ_0 is the background or reference density (1,025 kg m^{-3}); ρ is seawater density. Brunt-Väisälä frequency was calculated based on modeled data, and the maximum value, N^2_{max}, of a profile was used here to quantitatively represent the strength of bulk stratification.

3. Results

This coupled physical-biogeochemical model was previously implemented for this regions, and was found to well reproduce the observed temperature, salinity, bottom dissolved oxygen concentration (Zhang et al., 2018), and the pattern of surface chlorophyll (Zhang et al., 2021) in the East China Sea. The model-observation comparison of bottom oxygen is expanded to include 7 research cruises as listed in Table 1. Points generally distribute along the diagonal line although some split out slightly (Figure 3), with root-mean-square error $RMSE = 43.2$ mmol m^{-3}. The cruises were conducted in spring, summer, and fall seasons in different year, and observation stations distribute in both shallow and deep waters over the shelf. The point-to-point comparison implies this model ability in decently spatiotemporally reproducing the bottom oxygen concentration in the East China Sea.

This model decently reproduces the sea surface temperature (Figure 4) and captures the pattern of surface chlorophyll (Figure 5) in the Bohai and Yellow Seas. The 5-yr-August-averaged bottom temperature, salinity, and dissolved oxygen concentration in the Bohai and Yellow Seas (Figure 6) are compared to published observations
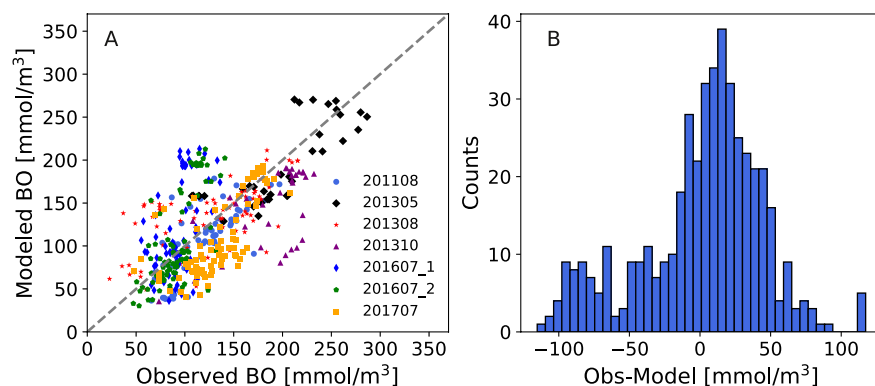
Figure 3. (a) Model-data point-to-point comparison of bottom oxygen in the East China Sea. (b) Histogram of observed oxygen concentration minus modeled (Obs-Model) oxygen concentration.
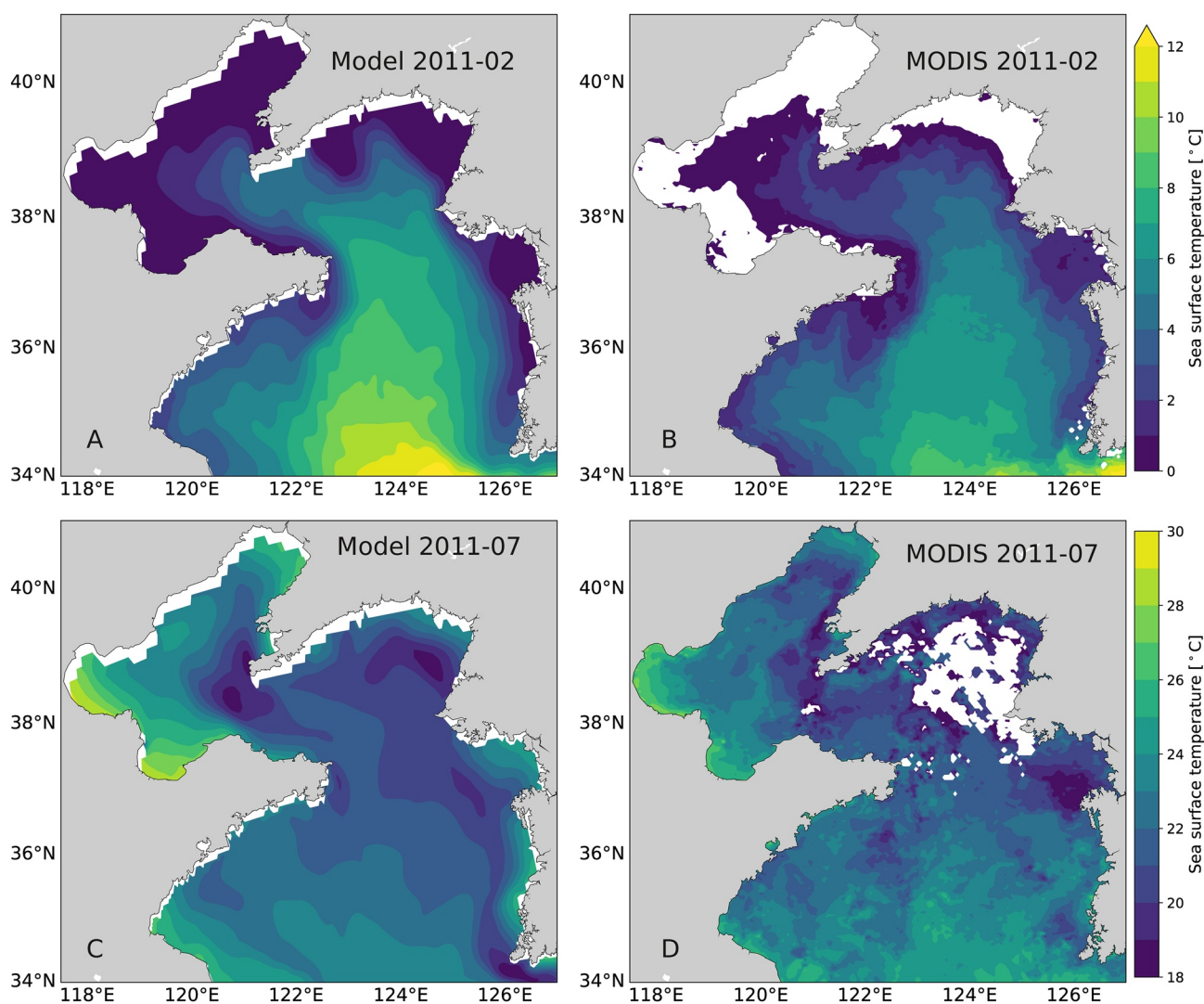

Figure 4. Comparison of sea surface temperature between modeled and satellite-derived results.
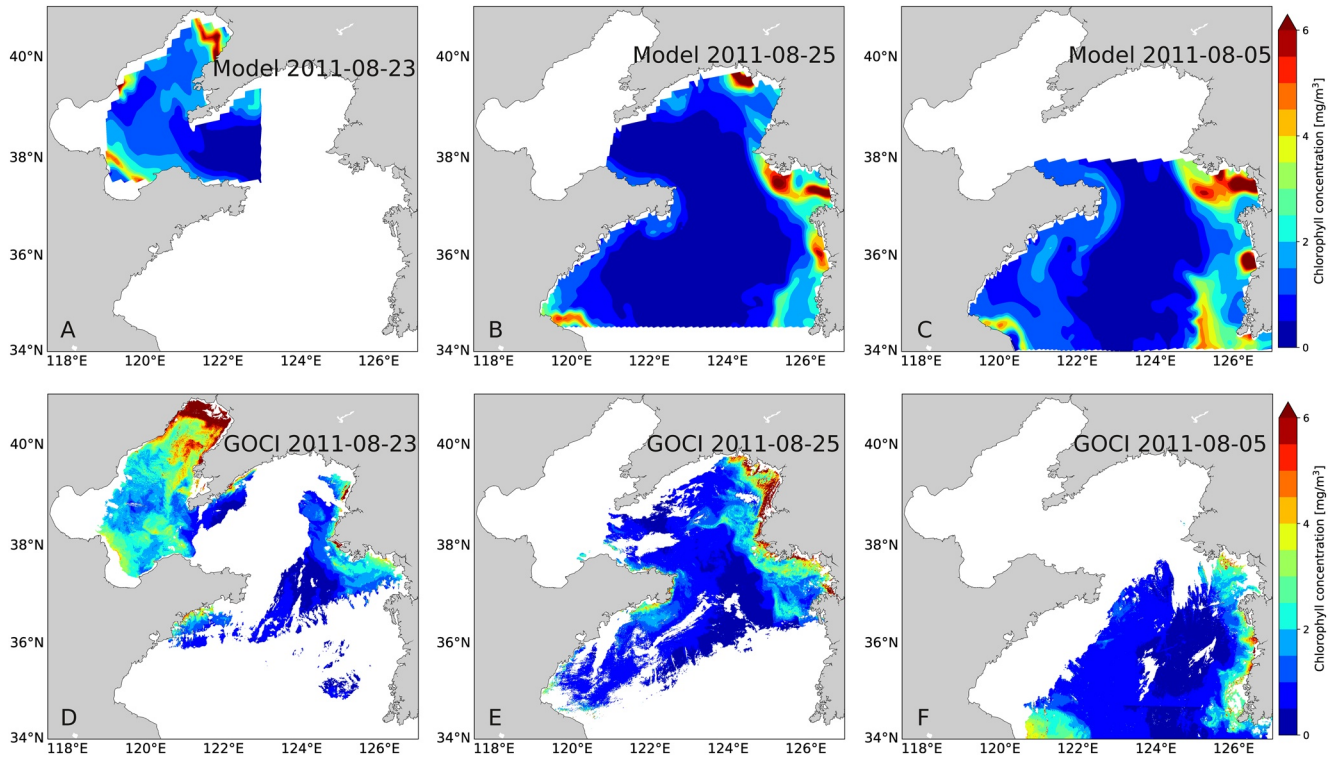
Figure 5. Comparison of surface chlorophyll concentration between modeled and satellite-derived results.

due to limited observation in hand. This model successfully captures the features of the Bohai Sea bottom temperature, salinity, and oxygen concentration (see Figure 2 in Wei et al., 2019). Bottom temperature is generally high along the coast and at the central shoal area, and low at deeper area (Figure 6a). Fresher areas along the coast are associated with the riverine freshwater input (Figure 6b), and the low bottom oxygen center locates at the offshore area of Qinhuangdao (Figure 6c). The Yellow Sea bottom cold water mass is well captured by the model (Figure 6a), with two cold cores locate at the north and south Yellow Sea, respectively (see Figure 10 in Yang et al., 2014). Bottom salinity is high in the south Yellow sea and decreases northward (see Figure 1 in Xiong et al., 2020) and cores of high bottom oxygen concentration (see Figure 3 in Xiong et al., 2020) generally are co-located with the cold cores (Figures 6a–6c). The validation implies that analysis based on this coupled model is reliable.

The bottom dissolved oxygen (averaged over the subregions as shown in Figure 1b) shows seasonal variations with high bottom oxygen concentration in winter and early spring seasons, and low bottom oxygen concentration in summer and early fall seasons (Figure 7a). The onset of bottom oxygen decrease generally occurs in late spring, and bottom oxygen reaches the annual minima by the end of summer/early fall season. Model results indicate that
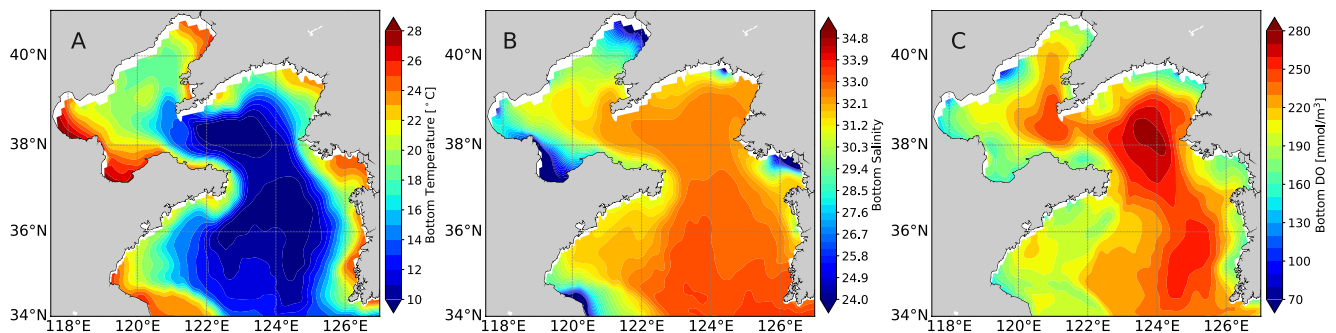

Figure 6. Plan-view of modeled (a) bottom temperature (b) bottom salinity, and (c) bottom dissolved oxygen in August.
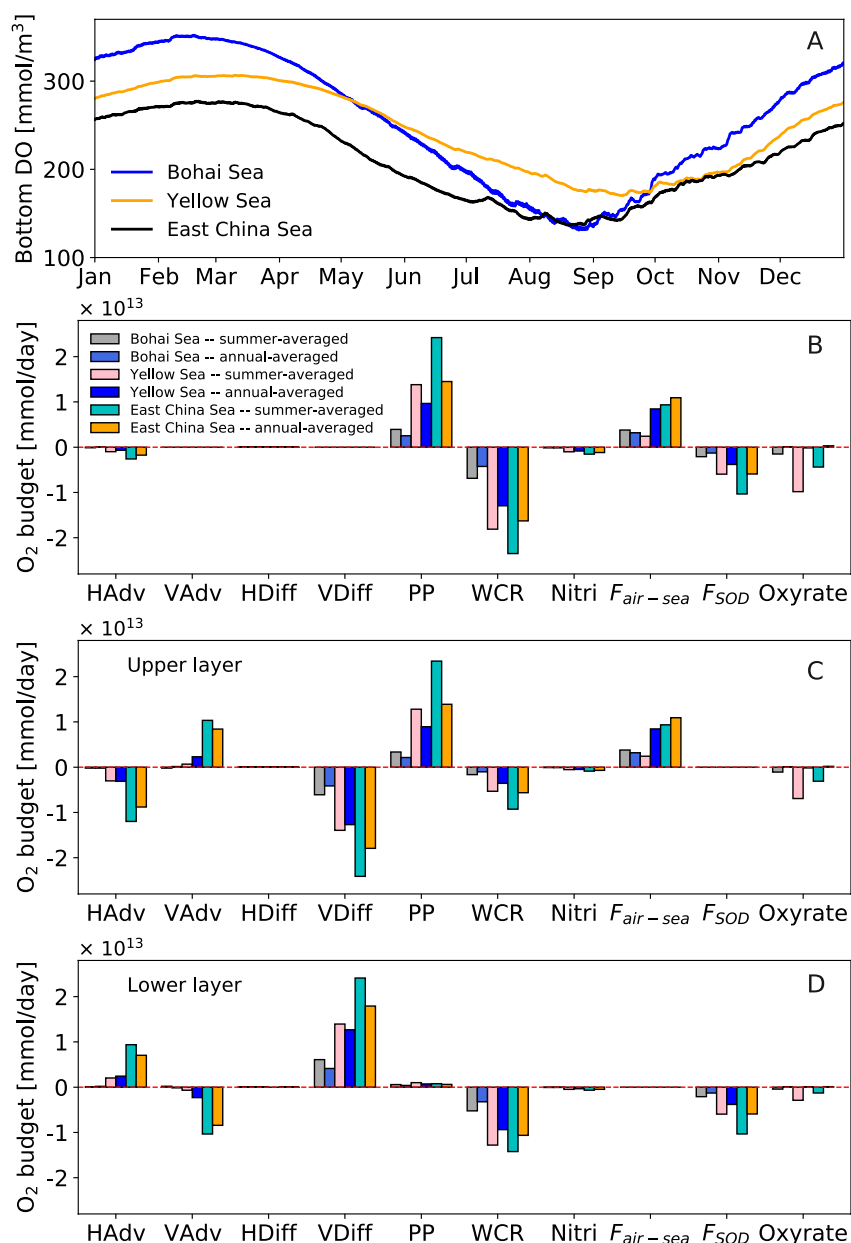
Figure 7. (a) Modeled annual cycle of bottom dissolved oxygen concentration. Oxygen budget for the Bohai Sea, Yellow Sea, and East China Sea for (b) the entire water column (c) the upper layer (the upper 70% of the water column), and (d) the lower layer (the lower 30% of the water column). Abbreviations on x-axis in panels B–D are for horizontal advection (*H*Adv), vertical advection (*V*Adv), horizontal diffusion (*H*Diff), vertical diffusion (*V*Diff), primary production (*PP*), nitrification (*Nitri*), air-sea flux ($F_{air-sea}$), sediment oxygen demand (F_{SOD}), water column respiration (*WCR*), and net change in oxygen concentration (*Oxyrate*). Note that F_{SOD} is zero in the upper layer and $F_{air-sea}$ is zero in the lower layer by definition.

the Bohai Sea bottom oxygen decrease occurs at a faster rate (larger decrease in the same time period), as shown in Figure 7a.

Oxygen budget analysis based on 2011–2015 averaged model data is done for the entire water column, the upper layer, and the lower layer (Figures 7b–7d). Note that positive value (source) in the budget means net gain of dissolved oxygen via certain process for the analyzed region while negative value (sink) means net loss of dissolved oxygen. Surface water gains dissolved oxygen via air-sea flux at the air-sea interface and primary production (Figures 7b and 7c) while near-bottom water losses dissolved oxygen via sediment oxygen demand at the water-seafloor interface and water column respiration (Figures 7b–7d). Vertical diffusion acts as an oxygen sink
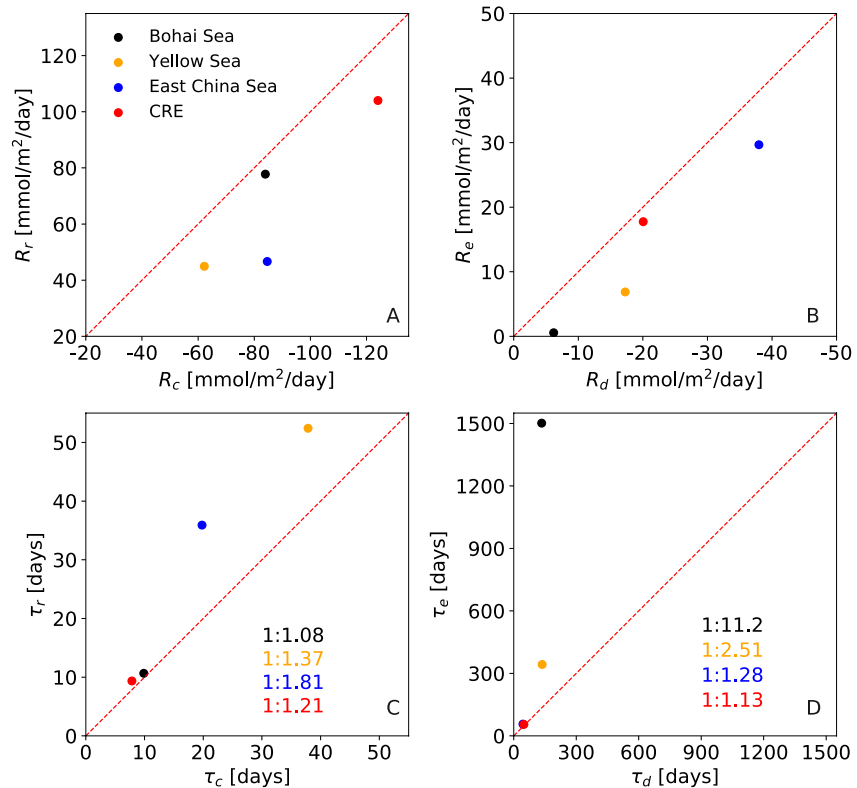
Figure 8. Comparisons for lower layer (a) normalized local oxygen consumption rate, R_c, and normalized replenishment rate, R_r (b) normalized local oxygen deficit rate, R_d, and normalized exchange rate, R_e (c) local oxygen consumption timescale, τ_c, and replenishment timescale, τ_r, and (d) local oxygen deficit timescale, τ_d, and exchange timescale, τ_e. Note that the ratios of timescales (τ_c–τ_r, τ_d,τ_e) are labeled for panels C and D, and the dashed red lines represent 1:1.

for the upper layer while as an oxygen source for the lower layer (Figures 7c and 7d). The annual-averaged net change in oxygen inventory (*Oxyrate*) is trivial among all subregions, which makes sense because the changes in dissolved oxygen inventory is expected to be balanced in an annual cycle, assuming no fundamental modifications are caused by climate change in one year. The oxygen inventory (integral of oxygen concentration) shows a net loss in summer which is reflected in the decline of oxygen concentration among all subregions (Figure 7).

Lower layer budget analysis is used to identify the roles that different budget terms play in the summer bottom oxygen decrease (Figure 7d). Lower layer budget indicates that *HAdv*, *VDiff*, and *PP* are oxygen sources, with the former one a lateral process, and the latter two local processes. The biogeochemical processes *WCR*, *Nitrif*, and F_{SOD} consume dissolved oxygen and act as local oxygen sinks. The process *VAdv* is a physical process that acts as local oxygen sink in the Yellow Sea and East China Sea while as local oxygen source in the Bohai Sea. Among all the oxygen budget terms, *HDiff*, *PP*, and *Nitrif* are small, with *HAdv*, *VAdv*, *VDiff*, *WCR*, and F_{SOD} predominant. On the other hand, both *HAdv* and *VAdv* are weak and considerably smaller in the Bohai Sea than in the other two subregions.

The rates and timescales of dissolved oxygen variation in the lower layer are compared among the three subregions to isolate the roles of local, vertical and lateral processes in seasonal bottom oxygen decrease (Figure 8). Note that bottom hypoxia generally occurs in summer, thus, the rates and timescales are quantified based on model summer results (Table 2).
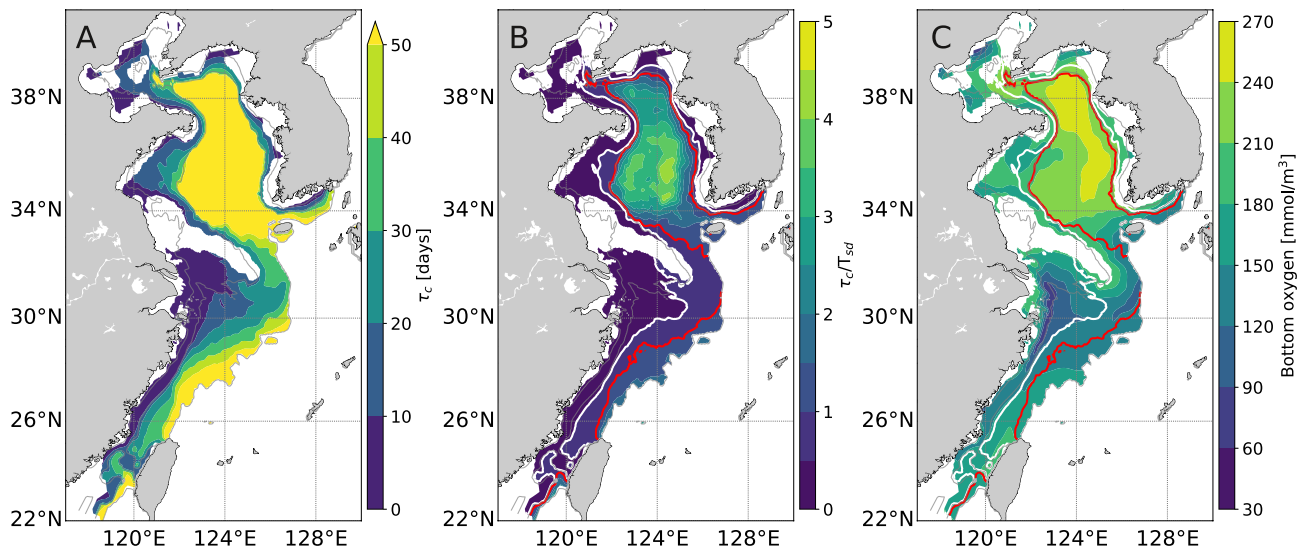
Table 2
Related Information for the Summer Timescales as Shown in Figures 8c, 8d

	Bohai sea	Yellow sea	East China sea	CRE
dz (m)	5.5	13.8	12.4	8.6
R_c (mmol m^{-2} day^{-1})	−84	−62.2	−84.6	−124.1
R_r (mmol m^{-2} day^{-1})	77.8	45	46.7	104
R_d (mmol m^{-2} day^{-1})	−6.2	−17.2	−38	−20
R_e (mmol m^{-2} day^{-1})	0.6	6.9	29.7	17.8
τ_c (day)	9.9	37.9	19.8	7.8
τ_r (day)	10.7	52	35.9	9.4
τ_d (day)	134.1	136.4	44.1	48.5
τ_e (day)	1,501.6	342.8	56.5	54.8

Note. The R_c, R_r, R_d, and R_e are the rates for local oxygen consumption, vertical oxygen replenishment, local oxygen deficit, and lateral oxygen exchange, respectively. The τ_c, τ_r, τ_d, and τ_e are the timescales for local oxygen consumption, vertical oxygen replenishment, local oxygen deficit, and lateral oxygen exchange, respectively. Note that dz is the spatial-averaged thickness of the lower layer in the three subregions, and the values for normalized variation rates are summer-average for the lower layer.

Figure 9. (a) Spatial distribution of τ_c (b) the ratio of τ_c and vertical stratification duration, T_{sd}, and (c) the summer-averaged bottom dissolved oxygen concentration. The white and red isolines in panels (b) and (c) represent $\tau_c/T_{sd} = 0.5$ and 1, respectively. The gray isolines are 20, 50, and 100 m isobaths. Note that the inshore well-mixed regions, vertical stratification duration $T_{sd} < 5$ days, are blanked.

In summer, local oxygen deficit often occurs with a faster bottom oxygen consumption rate than a vertical replenishment rate (Figure 8a), and the net oxygen decrease rate is determined by the competition between lateral exchange rate and local deficit rate (Figure 8b). The East China Sea shows the fastest local deficit rate among the three subregions, followed by the Yellow Sea, and the Bohai Sea shows the slowest local deficit rate (Table 2). However, the extremely slow lateral exchange rate between Bohai Sea and the other subregions (Table 2) could cause fast oxygen concentration drop in the lower layer of the Bohai Sea. For instance, the bottom oxygen concentration shows the fastest decrease rate in the Bohai Sea (Figure 7a). The bottom oxygen decrease rate in the Bohai sea is -5.6 mmol m^{-2} day^{-1} (the averaged thickness of the lower layer is 5.5 m, see Table 2), which is equivalent to 1.02 mmol m^{-3} day^{-1}. This rate is relatively slower compared to the observation-based bottom oxygen decrease rate, 2.18 mmol m^{-3} day^{-1}, in Song et al. (2020). The model-based rate is slower because it is a spatial-averaged rate over the entire Bohai Sea, and the value in Song et al. (2020) is derived from observations in a low-bottom-oxygen area of the Bohai Sea, in which oxygen decrease rate is much faster.

The ratios of local oxygen consumption timescale (τ_c) to vertical oxygen replenishment timescale (τ_r) are 1:1.81, 1:1.37, and 1:1.08 for the East China Sea, the Yellow Sea, and the Bohai Sea, respectively (Figure 8c). The ratios are close to the one-to-one line, indicating that the three subregions have one thing in common - comparable timescales for local consumption and vertical replenishment processes. In contrast, the ratios of local oxygen deficit timescale (τ_d) to lateral exchange timescale (τ_e) show large differences among the three subregions, 1:11.2, 1:2.51, and 1:1.28 for the Bohai Sea, the Yellow Sea, and the East China Sea, respectively (Figure 8d).

4. Discussion

Timescale analysis is an efficient approach to evaluate dissolved oxygen variation and bottom hypoxia formation. Fennel and Testa (2019) estimated the timescales of hypoxia and residence based on existing results from multiple regional systems. Shen et al. (2013) used a two-layer conceptual model based on the timescales of vertical exchange, horizontal advection, and biochemical consumption of dissolved oxygen to evaluate lower layer oxygen distribution in the Chesapeake Bay. This study uses a high resolution, coupled physical-biogeochemical model to simulate dissolved oxygen dynamics in the coastal seas in east China, which enabled us to investigate the roles of different physical and biogeochemical processes on oxygen seasonal variation.

Here we use the timescale of local oxygen consumption (Figure 9a), τ_c, to interpret the effectiveness and efficiency of timescale analysis. Both oxygen change rate and background oxygen condition determine the magnitude of timescale. The timescale of local oxygen consumption varies spatially and comparison of this timescale among

subregions indicates the differences of local biogeochemical features. The longer τ_c in the deep Yellow Sea is due to the high background dissolved oxygen condition as shown in Figure 6c. Short timescale indicates that the local biogeochemical feature is favorable for bottom hypoxia to form.

This timescale of local oxygen consumption, τ_c, combines with vertical stratification duration (unit in *day*) to give the bounds of hypoxia and non-hypoxia regions. The vertical stratification duration, T_{sd}, is defined as the accumulated time that $N^2_{\max}$ exceeds its summer-averaged value, and Figure 9b shows τ_c/T_{sd}. The vertical replenishment timescale, τ_r (controlled by *VAdv* and *VDiff*), is very patchy due to complex distribution of vertical component of shelf current. Hence, T_{sd} is used to simply represent replenishment timescale for this comparison. Following e-folding timescale principle, hypoxia is prone to form with $\tau_c/T_{sd} < 0.5$ while hypoxia is unlikely to form with $\tau_c/T_{sd} > 1$. Hence, seasonal hypoxia usually forms in coastal regions in east China seas that are confined within the white isoline ($\tau_c/T_{sd} = 0.5$) as shown in Figure 9b, with the maximum of τ_c being 25 days. In contrast, hypoxia is unlikely to occur in the deep Yellow Sea and offshore regions beyond the red isoline ($\tau_c/T_{sd} = 1$). Figure 9c shows that low bottom oxygen concentration is generally confined within the coastal regions while the oxygen concentration is high in the deep Yellow Sea and offshore regions. The above conclusions are consistent with the previous studies (Xomchuk et al., 2021)

Our method of timescale quantification and comparison can be used to understand the processes sustaining oxygen decrease and the occurrence of bottom hypoxia. Note that a subregion is considered as a whole hereafter and the discussion of timescale is based on Table 2 and Figure 8. Short τ_c (<25 days) is favorable for the occurrence of hypoxia. The relatively longer τ_c in the Yellow Sea indicates that hypoxia is unlikely to form there. Extremely long τ_e indicates that oxygen variation of the region is predominantly controlled by local processes, such as in the Bohai Sea and the Yellow Sea (Table 2).

Comparable τ_d and τ_e under short τ_c indicate that the local oxygen deficit can be rapidly remitted by supply through lateral exchange. Transient seasonal bottom hypoxia often forms under such circumstances, for instance, the duration of bottom hypoxic condition off the Changjiang River Estuary in the East China Sea is generally short, in the timescale of days (Zhang et al., 2018). The areal extent of bottom hypoxia varies significantly in the timescale of days (Figure 10 in Zhang et al. (2018)). In contrast, extremely long τ_e could cause long-lasting bottom hypoxia until the local seasonal oxygen deficit condition is relaxed. For instance, the bottom hypoxic condition in the Chesapeake Bay can last the whole summer and early fall seasons (Murphy et al., 2011). The Bohai Sea τ_e is over 10 times longer than its τ_d, indicating long-lasting low-bottom-oxygen under short τ_c in summer until the onset of strong cooling and mixing. This is consistent with Song et al. (2020), who observed persistent bottom oxygen decrease over the whole summer.

The ratio of τ_d and τ_e is insensitive to the domain size of a selected subregion so long as it includes the local hypoxic zone in its entirety (Figure 8). The Changjiang River Estuary (CRE) region, the area that is shallower than 50 m and seasonal hypoxia usually forms in the East China Sea, was analyzed and compared with the East China Sea subregion. The results are shown in Table 2 and Figure 8. The exact values of the corresponding rates change with the change of subregion spatial scale. For instance, the local oxygen consumption rate is faster in the CRE than that in the East China Sea subregion, this is because the impact of anthropogenic eutrophication is profound in the CRE region. In the Bohai Sea, the spatial-averaged bottom oxygen concentration decline (1.02 mmol m^{-3} day^{-1}) is slow compared to the bottom oxygen concentration decline in the low-bottom-oxygen area (2.18 mmol m^{-3} day^{-1}). The exact values of the corresponding timescales also change, such as the replenishment and local oxygen consumption timescales are much shorter in the CRE than in the East China Sea subregion (Figure 8c). These are consistent with the findings in Xomchuk et al. (2021) in which the relative importance of advection and diffusion could change at different spatial scales. The ratio of τ_c and τ_r changes from 1:1.81 in the East China Sea subregion to 1:1.21 in the CRE while the ratio of τ_d and τ_e shows minor change, from 1:1.28 to 1:1.13.

The quantification of these timescales is also important in informing efficient mitigation strategies for local ecosystem protection. In regions like the East China Sea with comparable τ_d and τ_e, processes that elongate τ_d can significantly mitigate bottom hypoxia expansion. A 30% abatement in the Changjiang riverine nutrient concentration significantly reduced the horizontal and vertical expansion of hypoxic water off the estuary, and the total volume of hypoxic water declined by 46% (Zhang et al., 2021), indicating more optimal space for fishes and other marine organisms. Regions like the Bohai Sea are under serious threat of severe seasonal bottom hypoxia.

Multiple stressors, like a warming climate and intense anthropogenic activities, working in parallel may worsen the situation by decreasing the bottom oxygen concentration minima and elongating the duration of bottom hypoxia.

More comprehensive strategies are required to stop the collapse of ecosystems under the threat of long-lasting, seasonal bottom hypoxia. Shellfish aquaculture is considered an efficient eutrophication abatement strategy (Bricker et al., 2018) because filter-feeding shellfish naturally removes organic matter. Artificial ventilation with pumps that can increase vertical replenishment (Stigebrandt et al., 2015) could also be considered as an efficient strategy to ease dissolved oxygen stress. Further investigations for the Bohai Sea are needed to further develop that can efficiently control bottom hypoxia expansion.

5. Conclusions

This study separates processes that can cause summer bottom oxygen variation into local, vertical and lateral processes. The rates and timescales for local consumption, vertical replenishment, local deficit, and lateral exchange are defined and quantified using oxygen budget analysis based on a couple physical-biogeochemical model for the coastal seas in east China. Hypoxia is prone to form under short timescale for local oxygen consumption ($\tau_c < 25$ days). The East China Sea, Yellow Sea, and Bohai Sea all have comparable τ_c and τ_r (timescale for vertical replenishment). In contrast, the ratios of τ_d (timescale for local oxygen deficit) to τ_e (timescale for oxygen lateral exchange) show large differences among the three subregions. Comparable τ_d to τ_e under short τ_c often yields transient seasonal bottom hypoxia to form, such as the East China Sea. Extremely long τ_e under short τ_c leads to long-lasting bottom hypoxia until the relaxation of local oxygen deficit condition, such as the Bohai Sea.

The definition of these timescales for bottom oxygen variation has general applicability to coastal seas worldwide. Quantitative comparison of these timescales in one region can isolate the contributions of biogeochemical processes induced local oxygen consumption, vertical physical replenishment, and supply by lateral exchange with offshore waters to seasonal bottom oxygen variation. Moreover, the comparison of the ratios of these timescales among regions can separate the sustainment of bottom hypoxia into transient and long-lasting features, and provide an important context for relative vulnerability to changes in nutrient and organic input and stratification under changing freshwater supply and climate warming. More comprehensive strategies like land use management, aquaculture, and artificial oxygen ventilation for regions under the threat of long-lasting bottom hypoxia are required to prevent the cause of irreversible consequences to local ecosystems.

Data Availability Statement

Required data are available at http://doi.org/10.5281/zenodo.5138965.

References

Breitburg, D. L., Levin, L. A., Oschlies, A., Grégoire, M., Chavez, F. P., Conley, D. J., et al (2018). Decling oxygen in the global ocean and coastal waters. *Science*, *359*. https://doi.org/10.1126/science.aam7240

Bricker, S. B., Ferreira, J. G., Zhu, C., Rose, J. M., Galimany, E., Wikfors, G., et al. (2018). Role of shellfish aquaculture in the reduction of eutrophication in an urban estuary. *Environmental Science & Technology*, *52*(1), 173–183. https://doi.org/10.1021/acs.est.7b03970

Brunt, D. (1927). The period of simple vertical oscillations in the atmosphere. *Quarterly Journal of the Royal Meteorological Society*, *53*(221), 30–32. https://doi.org/10.1002/qj.49705322102

Bryan, J. R., Riley, J. P., & Williams, P. J. (1976). A winkler procedure for making precise measurements of oxygen concentration for productivity and related studies. *Journal of Experimental Marine Biology and Ecology*, *21*, 191–197. https://doi.org/10.1016/0022-0981(76)90114-3

Carstensen, J., Andersen, J. H., Gustafsson, B. G., & Conley, D. J. (2014). Deoxygenation of the Baltic Sea during the last century. *Proceedings of the Natioanl Adademy of Sciences of the United States of America*, *111*(15), 5628–5633. https://doi.org/10.1073/pnas.1323156111

Chen, C.-C., Gong, G.-C., & Shiah, F.-K. (2007). Hypoxia in the East China Sea: One of the largest coastal low-oxygen areas in the world. *Marine Environmental Research*, *64*, 399–408. https://doi.org/10.1016/j.marenvres.2007.01.007

Conley, D. J., Carstensen, J., Aigars, J., & Axe, P.(2011). Hypoxia is increasing in the coastal zone of the Baltic Sea. *Environmental Science & Technology*, *45*(16), 6777–6783. https://doi.org/10.1021/es201212r

Conley, D. J., Carstensen, J., Vaquer-Sunyer, R., & Duarte, C. M. (2009). Ecosystem thresholds with hypoxia. *Hydrobiologia*, *629*, 21–29. https://doi.org/10.1007/s10750-009-9764-2

Egbert, G. D., & Erofeeva, S. Y. (2002). Efficient inverse modeling of barotropic ocean tides. *Journal of Atmospheric and Oceanic Technology*, *19*, 183–204. https://doi.org/10.1175/1520-0426(2002)019<0183:eimobo>2.0.co;2

Eppley, R. W. (1972). Temperature and phytoplankton growth in the sea. *Fish & Bull.*, *70*(4), 1063–1085

Evans, G., & Parslow, J. S. (1985). A model of annual plankton cycles. *Biological Oceanography*, *3*(3), 327–347

Fennel, K., Hetland, R., Feng, Y., & DiMarco, S. (2011). A coupled physical-biological model of the northern gulf of Mexico shelf: Model description, validation and analysis of phytoplankton variability. *Biogeosciences*, *8*, 1881–1899. https://doi.org/10.5194/bg-8-1881-2011

Fennel, K., Hu, J., Laurent, A., Marta-Almeida, M., & Hetland, R. (2013). Sensitivity of hypoxia predictions for the Northern Gulf of Mexico to sediment oxygen consumption and model nesting. *Journal of Geophysical Research: Oceans*, *118*, 990–1002. https://doi.org/10.1002/jgrc.20077

Fennel, K., & Testa, J. M. (2019). Biogeochemical controls on coastal hypoxia. *Annual Review of Marine Science*, *11*, 105–130. https://doi.org/10.1146/annurev-marine-010318-095138

Gao, L., Li, D., & Zhang, Y. (2012). Nutrients and particulate organic matter discharged by the Changjiang (Yangtze river): Seasonal variations and temporal trends. *Journal of Geophysical Research*, *117*. https://doi.org/10.1029/2012jg001952

Garcia, H. E., & Gordon, L. I. (1992). Oxygen solubility in seawater: Better fitting equations. *Limnology & Oceanography*, *37*, 1307–1312. https://doi.org/10.4319/lo.1992.37.6.1307

Hagy, J. D., Boynton, W. R., Keefe, C. W., & Wood, K. V. (2004). Hypoxia in chesapeake bay, 1950–2001: Long-term change in relation to nutrient loading and river flow. *Estuaries*, *27*(4), 634–658. https://doi.org/10.1007/bf02907650

Hetland, R. D., & DiMarco, S. F. (2008). How does the character of oxygen demand control the structure of hypoxia on the Texas-Louisiana continental shelf? *Journal of Marine Systems*, *70*, 49–62. https://doi.org/10.1016/j.marsys.2007.03.002

Kim, T.-W., K. Lee, Lee, C. K., Jeong, H. D., Suh, Y. S., Lim, W. A. (2013). Interannual nutrient dynamics in Korean coastal waters. *Harmful Algae*, *30*, 15–27. https://doi.org/10.1016/j.hal.2013.10.003

Laurent, A., Fennel, K., Cai, W.-J., Huang, W.-J., Barbero, L., & Wanninkho, R. (2017). Eutrophication-induced acidification of coastal waters in the northern Gulf of Mexico: Insights into origin and processes from a coupled physical-biogeochemical model. *Geophysical Research Letters*, *44*, 946–956. https://doi.org/10.1002/2016gl071881

Liu, X., Dunne, J. P., Stock, C. A., Harrison, M. J., Adcroft, A., & Resplandy, L. (2019). Simulating water residence time in the coastal ocean: A global perspective. *Geophysical Research Letters*, *46*(2313), 910919–911013. https://doi.org/10.1029/2019gl085097

Murphy, R. R., Kemp, W. M., & Ball, W. P. (2011). Long-term trends in chesapeake bay seasonal hypoxia, stratification, and nutrient loading. *Estuaries and Coasts*, *34*(6), 1293–1309. https://doi.org/10.1007/s12237-011-9413-7

Najjar, R. G., Herrmann, M., Alexander, R., Boyer, E. W., Burdige, D., Butman, D., et al. (2018). Carbon budget of tidal wetlands, estuaries, and shelf waters of eastern north America. *Global Biogeochemical Cycles*, *32*(3), 389–416. https://doi.org/10.1002/2017gb005790

Ni, X., Huang, D., Zeng, D., Zhang, T., Li, H., & Chen, J., et al (2016). The impact of wind mixing on the variation of bottom dissolved oxygen off the Changjiang Estuary during summer. *Journal of Marine Systems*, *154*, 122–130. https://doi.org/10.1016/j.jmarsys.2014.11.010

Rabalais, N. N., Diaz, R. J., Levin, L. A., Turner, R. E., Gilbert, D., & Zhang, J. (2010). Dynamics and distribution of natural and human-caused coastal hypoxia. *Biogeosciences*, *7*, 585–619. https://doi.org/10.5194/bg-7-585-2010

Rabalais, N. N., Turner, R. E., & Wiseman, W. J., Jr (2001). Hypoxia in the gulf of Mexico. *Journal of Environmental Quality*, *30*(2), 320–329. https://doi.org/10.2134/jeq2001.302320x

Rabalais, N. N., Turner, R. E., & Wiseman, W. J., Jr (2002). Gulf of Mexico hypoxia, aka "the dead zone". *Annual Review of Ecology and Systematics*, *33*(1), 235–263. https://doi.org/10.1146/annurev.ecolsys.33.010802.150513

Shchepetkin, A. F., & McWilliams, J. C. (2005). The regional oceanic modeling system (ROMS): A split-explicit, free-surface, topographically-following-coordinate oceanic model. *Ocean Modelling*, *9*, 347–404. https://doi.org/10.1016/j.ocemod.2004.08.002

Shen, J., Hong, B., & Kuo, A. Y. (2013). Using timescales to interpret dissolved oxygen distributions in the bottom waters of Chesapeake Bay. *Limnology & Oceanography*, *58*(6), 2237–2248. https://doi.org/10.4319/lo.2013.58.6.2237

Song, G., Zhao, L., Chai, F., Liu, F., Li, M., & Xie, H. (2020). Summertime oxygen depletion and acidification in Bohai sea, China. *Frontiers in Marine Science*, *7*, 252. https://doi.org/10.3389/fmars.2020.00252

Stigebrandt, A., Rosenberg, R., Råman Vinnå, L., & Ödalen, M. (2015). Consequences of artificial deepwater ventilation in the Bornholm basin for oxygen conditions, cod reproduction and benthic biomass–a model study. *Ocean Science*, *11*(1), 93–110. https://doi.org/10.5194/os-11-93-2015

Takeoka, H. (1984). Fundamental concepts of exchange and transport time scales in a coastal sea. *Continental Shelf Research*, *3*(3), 311–326. https://doi.org/10.1016/0278-4343(84)90014-1

Wang, Y., Wu, H., Lin, J., Zhu, J., Zhang, W., & Li, C. (2019). Phytoplankton blooms off a high turbidity estuary: A case study in the Changjiang river estuary. *Journal of Geophysical Research: Oceans*, *124*, 8036–8059. https://doi.org/10.1029/2019jc015343

Wanninkhof, R. (2014). Relationship between wind speed and gas exchange over the ocean revisited. *Limnology & Oceanography*, *12*, 351–362. https://doi.org/10.4319/lom.2014.12.351

Wei, Q., Wang, B., Yao, Q., Xue, L., Sun, J., Xin, M., & Yu, Z. (2019). Spatiotemporal variations in the summer hypoxia in the Bohai sea (China) and controlling mechanisms. *Marine Pollution Bulletin*, *138*, 125–134. https://doi.org/10.1016/j.marpolbul.2018.11.041

Wiseman, W. J., Jr, Rabalais, N. N., Turner, R. E., Dinnel, S. P., & MacNaughton, A. (1997). Seasonal and interannual variability within the Louisiana coastal current: Stratification and hypoxia. *Journal of Marine Systems*, *12*, 237–248. https://doi.org/10.1016/s0924-7963(96)00100-5

Xiong, T.-q., Wei, Q.-s., Zhai, W.-d., Li, C.-l., Wang, S.-y., Zhang, Y.-x., et al. (2020). Comparing subsurface seasonal deoxygenation and acidification in the yellow sea and northern east China sea along the north-to-south latitude gradient. *Frontiers in Marine Science*. https://doi.org/10.3389/fmars.2020.00686

Xomchuk, V. R., Hetland, R. D., & Qu, L. (2021). Small-scale variability of bottom oxygen in the northern Gulf of Mexico. *Journal of Geophysical Research: Oceans*, *126*. https://doi.org/10.1029/2020jc016279

Yang, H.-W., Cho, Y.-K., Seo, G.-H., You, S. H., & Seo, J.-W. (2014). Interannual variation of the southern limit in the yellow sea bottom cold water and its causes. *Journal of Marine Systems*, *139*, 119–127. https://doi.org/10.1016/j.jmarsys.2014.05.007

Yu, L., Fennel, K., & Laurent, A.(2015). A modeling study of physical controls on hypoxia generation in the northern Gulf of Mexico. *Journal of Geophysical Research: Oceans*, *120*, 5019–5039. https://doi.org/10.1002/2014jc010634

Zhang, W., Hetland, R. D., Ruiz, V., DiMarco, S. F., & Wu, H. (2020). Stratification duration and the formation of bottom hypoxia over the Texas-Louisiana shelf. *Estuarine, Coastal and Shelf Science*, *238*. https://doi.org/10.1016/j.ecss.2020.106711

Zhang, W., Moriarty, J., Wu, H., & Feng, Y. (2021). Response of bottom hypoxia off the Changjiang river estuary to multiple factors: A numerical study. *Ocean Modelling*, *159*, 101751. https://doi.org/10.1016/j.ocemod.2021.101751

Zhang, W., Wu, H., Hetland, R. D., & Zhu, Z. (2019). On mechanisms controlling the seasonal hypoxia hotspots off the Changjiang River estuary. *Journal of Geophysical Research: Oceans*, *124*, 8683–8700. https://doi.org/10.1029/2019jc015322

Zhang, W., Wu, H., & Zhu, Z. (2018). Transient hypoxia extent off Changjiang river estuary due to mobile Changjiang river plume. *Journal of Geophysical Research: Oceans*, *123*(12), 9196–9211. https://doi.org/10.1029/2018jc014596

Zhou, F., Chai, F., Huang, D., Xue, H., Chen, J., Xiu, P., et al (2017). Investigation of hypoxia off the Changjiang Estuary using a coupled model of ROMS-CoSiNE. *Progress in Oceanography*, *159*, 237–254. https://doi.org/10.1016/j.pocean.2017.10.008